INORGANIC CHEMISTRY FRONTIERS

CCS 中国化学会 CHINESE CHEMICAL SOCIETY

ROYAL SOCIETY OF CHEMISTRY

Green Synthesis of Zr-Based Metal-Organic Framework Hydrogel Composites and Their Enhanced Adsorptive Properties

Journal:	*Inorganic Chemistry Frontiers*
Manuscript ID	QI-RES-07-2020-000840.R2
Article Type:	Research Article
Date Submitted by the Author:	21-Sep-2020
Complete List of Authors:	Klein, Shirell; California State University Los Angeles, Department of Chemistry and Biochemistry Sosa, Joshua; California State University Los Angeles, Department of Chemistry and Biochemistry Castonguay, Alexander; Pennsylvania State University, Department of Chemistry Flores, Willmer; California State University Los Angeles, Department of Chemistry and Biochemistry Zarzar, Lauren; Pennsylvania State University, Materials Science and Engineering Liu, Yangyang; California State University Los Angeles, Department of Chemistry and Biochemistry

ARTICLE

Green Synthesis of Zr-Based Metal-Organic Framework Hydrogel Composites and Their Enhanced Adsorptive Properties

Received 00th January 20xx,
Accepted 00th January 20xx

DOI: 10.1039/x0xx00000x

Shirell E. Klein,[a] Joshua D. Sosa,[a] Alexander C. Castonguay,[b] Willmer I. Flores,[a] Lauren D. Zarzar,* [bcd] and Yangyang Liu* [a]

Metal-organic frameworks (MOFs) have emerged as promising candidates for a wide range of applications due to their high surface area and customizable structures, however, the minimal external hydrophilicity of MOFs has limited their biomedical implementations. Structuring of MOFs within polymer frameworks is an approach used to create hybrid materials that retain many of the MOF characteristics (e.g. high adsorption capacity) but expand the range of mechanical and surface properties as well as form factors accessible. Using this approach, hybridizing MOFs with hydrophilic hydrogels can give rise to materials with improved hydrophilicity and biocompatibility. Here, we describe the synthesis of the first Zr-based MOF-hydrogel hybrid material (composite **3**) using a green chemistry approach, in which only water was used as the solvent and relatively low temperature (50 °C) was applied. Using methylene blue (MB) as a probe molecule, composite **3** exhibited greater adsorption capacity than the MOF or the hydrogel alone in aqueous solution at most tested pH values (all except pH 13). At an initial MB concentration of 0.0096 mg/mL (30.014uM) and neutral pH conditions, this new hybrid presented the highest loading of MB among similar materials (MB adsorbed = 4.361 ± 0.092 mg MB/g Zr, partition coefficient = 0.172 ± 0.004 mg/g/uM) and largely retained its adsorption capacity under varied conditions (pH 1-13 and 0.2-1.0M NaCl), rendering possible applications in drug delivery and the removal of tumor contrast agent/dye with minimal leakage due to its broad chemical stability.

Introduction

Emergent challenges in diagnostics and biomedicine have promoted the development of new materials with superior loading capacity, broad chemical resistance, and precise target specificity. In particular, materials with unique adsorption properties are desired when it comes to the design of on-demand drug delivery systems.[1] Such materials often require hydrophilicity to improve blood compatibility, prevent protein adsorption, and facilitate adhesion to target cells.[2] Additionally, for *in vivo* implementation, materials with wide pH stability are of interest to withstand localized deviations from physiological pH, such as in the environment surrounding cancerous cells.[3] Organic drug delivery systems (e.g. polymers, lysosomes) offer exceptional biocompatibility,[4,5] and, consequently, organic polymers such as hydrogels have been investigated for use in advanced wound healing, immunology, and oncology with low risk of drug denaturation or aggregation.[6] However, these materials often lack the desired loading capacity provided by inorganic systems such as pure metal, metal-oxide, and silica-coated nanoparticles.[7-10] Therefore, hybrid materials that possess both low toxicity and high porosity have gained increasing attention in recent years with the synthesis of aerogels,[11,12] sol-gels,[13,14] and other semi-crystalline compounds as well as crystalline inorganic complexes including zeolites[15,16] and metal-organic frameworks (MOFs).[17,18]

MOFs are a class of highly crystalline materials that are composed of metal nodes and organic linkers.[19,20] Due to their high surface area, permanent porosity, thermal and chemical stability, as well as tailorable structure and functionality,[21-24] MOFs have become promising candidates for a wide range of applications, such as drug delivery,[25] catalysis,[26,27] gas storage,[28] and solar cells.[29] Nevertheless, powdered MOFs or compressed MOF pellets have poor conformational flexibility and limited direct biomedical applications due to their rigid structure and minimal external hydrophilicity of most MOFs, which can inhibit free circulation of MOF suspensions in aqueous solution and lead to particle aggregation.[30,31] Hydrophilic polymers, such as polyethylene glycol (PEG), have been post-synthetically modified onto MOF surfaces to improve their hydrophilicity and prevent agglomeration, but this method often requires cumbersome multi-step synthesis and only applies to certain MOFs with accessible modification sites.[32] Inversely, various MOF hybrids have also been prepared by functionalizing polymer or metal oxide substrates with MOF surfaces via post-synthetic modifications.[33-36] This approach is limited by the need for MOF processing before deposition, and/or the resultant composites tend

[a] *Department of Chemistry and Biochemistry, California State University Los Angeles, 5151 State University Dr, Los Angeles, CA 90032, United States*
[b] *Department of Chemistry, Pennsylvania State University, University Park, PA 16802, United States*
[c] *Department of Materials Science and Engineering, Pennsylvania State University, University Park, PA 16802, United States*
[d] *Materials Research Institute, Pennsylvania State University, University Park, PA 16802, United States*

Electronic Supplementary Information (ESI) available: Additional GS, PXRD, TGA, SEM, FTIR, and EDS characterization of synthesized materials and supporting dye adsorption experiments. See DOI: 10.1039/x0xx00000x

to lack structural continuity as the MOFs were incorporated as individual particles.[37-40] Additionally, the gelation of MOFs has been achieved by altering solvent ratios in the solvothermal synthesis, but the gelated MOFs tend to lack porosity and loading capacity needed for guest encapsulation.[41] On the other hand, internal incorporation of MOFs in gel substrates can give rise to new composites that combine the advantageous properties of both materials (i.e. superior loading capacity of MOFs and hydrophilicity of gels). Recently, Zhu et al. reported the synthesis of hybrids that embed MOF components within the cross-linking of highly stretchable and adaptive alginate hydrogels, which allowed for continuous large-scale structuring of MOFs within conformationally adaptive materials without requiring initial preparation of MOF particles.[42] A subsequent study explored the efficacy of water treatment applications for such MOF-alginate hydrogel hybrids, but the vast combinations for these materials are still largely undocumented.[43] To date, very little research has been done on the properties of these MOF-hydrogel hybrids,[44-46] such as their stimuli-responsiveness, relative adsorption capabilities of guest molecules, and potential biomedical applications. Furthermore, there have been no reports on the synthesis of Zr-based MOF-Alg composites, despite the great diversity and exceptional stability of Zr-based MOFs.[23] Given the low toxicity and high porosity of Zr-MOFs, hybridizing them with hydrogels can further improve their hydrophilicity and biocompatibility, which will promote their practical applications as efficient topical or injectable drug delivery platforms.[47,48]

Herein, we outline a green chemistry route to synthesize a new Zr-MOF-Alg composite, which uses only water as the solvent and requires relatively low temperature heating (50 °C). Remarkably, the obtained composite presented superior adsorptive properties compared to the MOF or the hydrogel alone, and it achieved the highest adsorption capacity of methylene blue (MB) in aqueous solution among similar materials.[42] MB was selected as a probe/model compound due to its reported applications in tumor targeting and imaging.[49,50] The synthesized composite also retained its superior adsorption capacity across pH 1-13, and its robustness may aid in MB removal when used as a contrast agent for tumor imaging, where extracellular regions are characteristically acidic (reaching below pH 5.5).[4] Essentially, taking advantage of the high loading capacity of MOFs and the hydrophilicity of hydrogels, this hybrid material offers an efficient novel platform for the delivery of therapeutics and/or the removal of excess dye molecules for bioimaging.

Experimental Section

Materials

Zirconyl chloride octahydrate (98+%), alginic acid sodium salt (viscosity: 15-25 cP -- 1% in H_2O), *N,N'*-Dimethylformamide (99.8+%), formic acid (98+%) and 1,3,5-benzenetricarboxylic acid or trimesic acid (98%) were purchased from ACROS Organics, methylene blue (high purity, biological stain) was purchased from Sigma-Aldrich, sodium hydroxide pellets (98.9+%), sodium chloride (99.0+%), hydrochloric acid (34-37% HCl), acetone (99.5+%) and ethanol (99.8+%) was purchased from Fisher Scientific. All reagents were used without further purification and all water used was deionized water.

Instrumentation

Powder X-ray diffraction (PXRD) patterns were collected on a Bruker D2 Phaser. Samples were scanned at 30 kV and 10 mA using a step size of $2\boldsymbol{\theta}$=0.01° (1.00 s per step) over a $2\boldsymbol{\theta}$ range of 5 to 30°. Thermogravimetric analysis (TGA) was done on a TA TGA 55 with a step size of 5.0 ℃/min over a range of 25 to 575 ℃. The instrument was calibrated with solid Sn weights at 10, 100, and 1000 mg. UV-visible (UV-vis) spectra were collected on a UV-1800 Shimadzu UV Spectrophotometer. A methylene blue dye calibration curve was created using 0.0008, 0.0016, 0.004, 0.008, 0.016, and 0.04 mg/mL methylene blue solutions (Figure S1). Gas sorption analyses were carried out with an Autosorb iQ-XR GS Analyzer. MOF-808 was activated at 150 ℃ for 24 hours before obtaining an N_2 isotherm. Supercritical CO_2 drying was performed using a samdri-PVT-3D dryer with bone-dry CO_2. SEM imaging was collected with a FEI Nova NanoSEM 630 SEM. Accelerating voltages of either 5 keV or 7 keV were used for imaging based on charge build up and EDS was obtained at 15 keV. A 5 nm coating of iridium metal was sputtered on all samples to improve static dissipation.

Zirconium Alginate (Zr-Alg) Cross-Linked Hydrogels

3 mL of a 10 mg/mL aqueous solution of sodium alginate was added dropwise to 15 mL of a 30 mg/mL $ZrOCl_2$ aqueous solution to form hydrogel beads with ~3 mm diameter, in quantities of approximately 30 beads per milliliter alginate. The mixture was stirred while the alginate solution was added, and the mixture was allowed to sit for 48 hours to ensure complete incorporation of zirconium into the hydrogels. The supernatant solution was decanted and Zr-Alg hydrogel beads were washed with water (3x15 mL).

Zr-MOF-Alg Composites

Three composites were synthesized by varying the synthetic conditions. Composite **1** was synthesized by adding the Zr-Alg hydrogels to 30 mg/mL trimesic acid ethanol solution, and the mixture was incubated at 85 ℃ in a closed container under pressure for 24 hours for MOF growth. This synthesis of composite **1** was adapted from Zhu et al.'s reported procedures on the synthesis of Cu^{2+}, Co^{2+}, Zn^{2+}, and Fe^{3+} MOF-Alg composites.[42] Composite **2** was synthesized under similar conditions but using only water as the solvent. Both composite **1** and **2** had low structural stability and fell apart upon removal from incubation following synthesis (Figure S2). Therefore, composite **3** was obtained using a green chemistry approach, in which we used only water as the solvent and a mild heating temperature. In detail, 450 mg trimesic acid was dissolved in 15 mL water, followed by adding the Zr-Alg hydrogels into the solution and incubating the mixture at 50 ℃ for 48 hours. Resultant Zr-MOF-Alg composite (**3**) beads were washed with water (3x15 mL) to remove excess trimesic acid. Only composite **3** was used for further testing due to its enhanced stability.

MOF-808

MOF-808 particles were synthesized following a procedure similar to that reported by Furukawa et al., in which 0.11 g trimesic acid and 0.16 g $ZrOCl_2 \cdot 8H_2O$ were dissolved in 40 mL of a 1:1 volume mixture of *N, N'*-dimethylformamide (DMF) and formic acid.[51] The mixture was then incubated at 100 ℃ for seven days before collecting the white crystals and washing with DMF (3x15 mL) and acetone (3x15 mL). The product was dried in a vacuum oven before activation under high vacuum at 150 ℃ for 24 hours (Yield: 0.087 g, 62% based on Zr). A nitrogen isotherm, powder X-ray diffraction (PXRD), thermogravimetric analysis (TGA), and scanning electron microscopy (SEM) were obtained for characterizations (Figure S3, S4d, S5a, S6).

Dye Removal Studies

Synthesized materials (Zr-Alg hydrogel/composite **3**/MOF-808) were immersed in methylene blue (MB) solutions of varying pH or varying ionic strength, each with a total volume of 10 mL containing 6 mL of 0.0096 mg/mL aqueous MB solution. The remaining 4 mL were used to obtain the desired solution pH. Ionic strength was altered by directly adding NaCl to the solution. Samples were allowed to soak in MB for 5 days to reach equilibrium (Figure S7), and UV-vis of the supernatant was then measured with a UV-1800 Shimadzu UV Spectrophotometer.

Results and Discussion

By varying the synthetic conditions as described in the Experimental Section, three Zr-MOF-Alg composites **1, 2** and **3** were obtained. Composites **1** and **2** were synthesized following an adapted procedure from literature.[42] Composite **3** was synthesized via a greener approach (Figure 1a), in which Zr-Alg hydrogels were first synthesized as previously described (Experimental Section) and the resultant semi-transparent white spherical beads (Figure 1b, right vial) were then further reacted with trimesic acid to obtain the opaque white beads of composite **3** (Figure 1b, left vial). Figure 1a presents the schematic of the green synthesis. In the synthesis of the Zr-Alg hydrogels, Zr^{4+} ions interact with sodium alginate, forming an "egg-box" cross-linked structure (Figure 1a, Zr-Alg hydrogels).[51] It was assumed that all Zr^{4+} used in the synthesis was incorporated into the gels during this process. This assumption was based on the equal dye adsorption in samples with varying alginate concentrations, indicating that the zirconium was the limiting reagent during crosslinking (Figure S8c). When Zr-Alg hydrogels reacted with trimesic acid under hydrothermal conditions at 50 °C, some of the Zr^{4+} in the hydrogels self-assembled with the trimesic acid linker to form porous MOF-like structures embedded within the hydrogel (Figure 1a, Zr-MOF-Alg composites).[42] Composite **3** was selected for further testing due to its greater observed structural stability and adsorptive capacity (Figure S2, S8). In order to analyze the structures of the obtained materials, composite **3** and the Zr-Alg hydrogels were dried using a supercritical CO_2 dryer, after which the adsorption capacity of the materials was mostly retained (Figure S8, S9). The dried samples were then analyzed using various techniques to confirm the proposed MOF-hydrogel hybrid structure. Firstly, the MOF linker (trimesic acid) incorporation was confirmed by FT-IR, which showed zirconium coordination to both trimesic acid and alginate linkers through red-shifting of the Zr-O (755 cm^{-1}) and C=O (1723 cm^{-1}) stretches, respectively (Figure S10). Secondly, a greater surface area was observed for composite **3** than the Zr-Alg hydrogels in gas sorption experiments, indicating the MOF component was indeed incorporated into the composites and created additional micropore surfaces (Figure S11). Thirdly, in thermogravimetric analysis (TGA), the weight loss corresponding to the decomposition of trimesic acid (starting ~500 K) was observed in both MOF-808 and composite **3**, but not Zr-Alg hydrogel (Figure S5). This further confirmed the successful incorporation of trimesic acid into composite **3.**

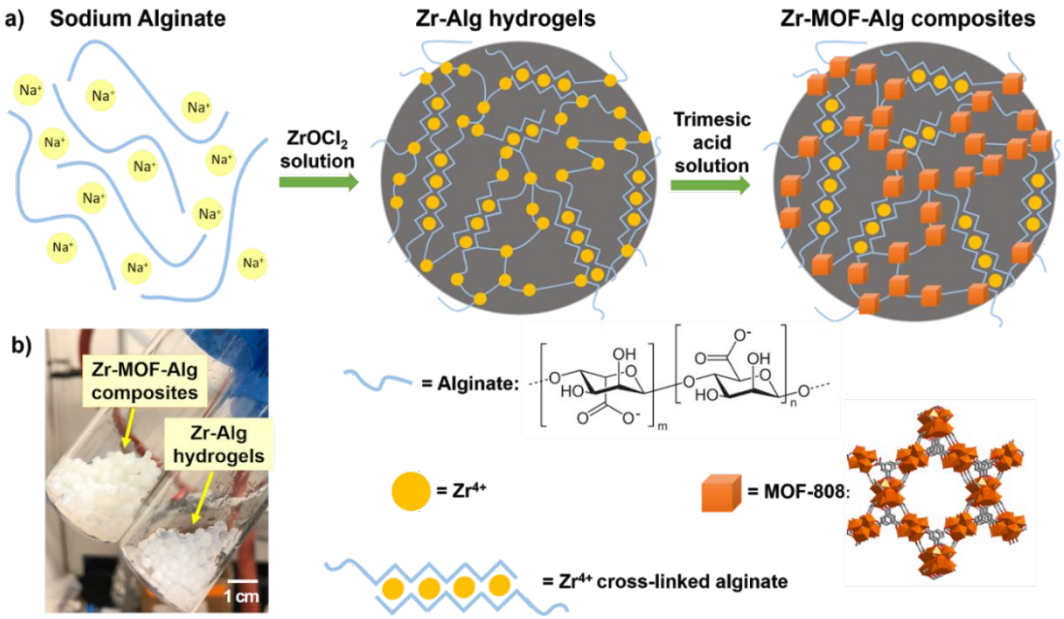

Figure 1 (a) Schematic of the preparation and proposed structures for Zr-Alg hydrogel and Zr-MOF-Alg composite. (b) Photographs of Zr-MOF-Alg composite **3** (left) and Zr-Alg hydrogel beads (right). Schematics are not drawn to scale.

Figure 2a/e present photographs of the as-synthesized gel beads of Zr-Alg hydrogel and composite **3**, respectively. After supercritical CO_2 drying, the morphology of both materials was studied by scanning electron microscopy (SEM). As shown in Figure 2b/f, compared to the as-synthesized samples, the diameter of the beads shrank by half upon drying for both Zr-Alg hydrogel and composite **3**, but their spherical shape was conserved. Using the weight of the supercritical CO_2 dried gels, swelling ratios of 28.263 and 20.030 were calculated for the composite and hydrogel, respectively. These ratios exhibit the tendency of the composite to swell more in aqueous solution compared to the hydrogel. Visible in the cross-section SEM image of Zr-Alg (Figure 2d), a porous structure was evident within the dried hydrogel. The cross-section SEM image of composite **3** presented a similar porous structure but with smaller voids, suggesting additional crosslinking with trimesic acid could be present in the composite (Figure 2h). Energy dispersive X-ray spectroscopy (EDS) mapping of the cross-sections was used to confirm an even distribution of zirconium throughout the samples of both Zr-Alg hydrogel and composite **3** (Figure S12).

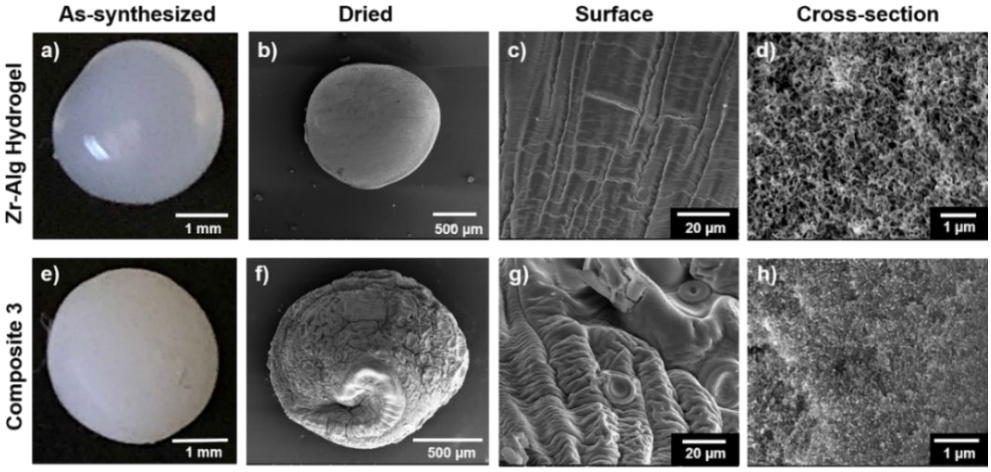

Figure 2 Photographs of as-synthesized Zr-Alg hydrogel (a) and composite **3** (e) gel beads. SEM images of supercritical CO_2 dried Zr-Alg hydrogel bead (b: whole bead, c: surface of bead, and d: cross-section of the bead) and composite **3** (f: whole bead, g: surface of the bead, and h: cross-section of the bead).

Having characterized the chemical structure of the synthesized materials, we next examined the adsorption capacity of composite **3** using MB as a probe molecule. In this experiment, composite **3** gels were immersed in 10 mL aqueous MB solution for 5 days and the concentration change of the MB supernatant solution was monitored by UV-vis. The amount of MB adsorbed by the composite was calculated based on the milligrams of MB being removed per gram of zirconium content in each sample. Proper MB saturation was determined by constructing an adsorption curve, using initial MB concentrations of 3.001uM, 15.007uM, 30.014uM, and 90.042uM (Figure 3a). The 30.014uM initial concentration corresponded to a relatively low saturation of the composite, and the adsorption at 90.042uM therefore provides a point for comparison with an initial MB concentration that is closer to full saturation of the adsorbent. Given the correlation of initial sorbent concentration to loading capacity and low MB concentrations in real world applications, 30.014uM MB concentration was used for further testing. The additional metric of partition coefficient (PC) was also calculated to assess the objectivity of MB adsorption values.[52] After scaling MB adsorption with the final MB concentration (in the supernatant), similar overall encapsulation trends were observed with more defined adsorption dependence (Figure 3b, Table 1). Figure 3b also highlighted the non-linear relationship between the initial MB concentration and the PC values. For consistency and ease of comparison with previous studies, MB adsorption in the form of mg MB/g Zr was used for subsequent plots. Tabulated PC values are shown for all samples in the SI (Table S1).

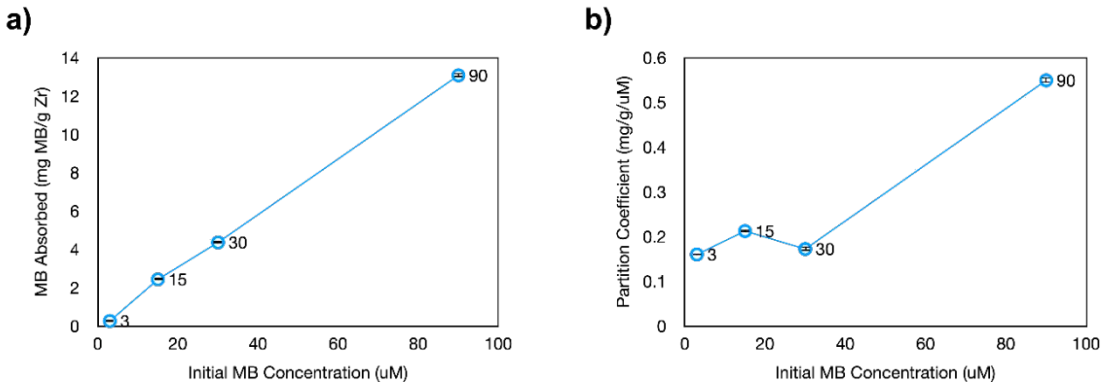

Figure 3 MB adsorption capacity of composite **3** at varied initial MB concentration with (a) MB adsorbed metric and (b) Partition coefficient (PC) metric (all samples performed in triplicate, shown as average with standard deviation for error). PC was calculated as mg MB adsorbed per g Zr partitioned from uM MB remaining in the supernatant.

Table 1 MB adsorption capacity of composite **3** at varied initial MB concentrations (all samples performed in triplicate, shown as average with standard deviation for error). PC is used to analyze the objectivity of the MB adsorbed metric by providing a contrasting scaled value.

Sample	Initial Concentration (uM MB)	Final Concentration (uM MB)	MB Adsorbed (mg MB/g Zr)	PC (mg/g/uM)
Composite 3	3.001	1.631	0.261 ± 0.013	0.160 ± 0.008
Composite 3	15.007	11.448	2.431 ± 0.072	0.212 ± 0.006
Composite 3	30.014	25.326	4.361 ± 0.092	0.172 ± 0.004
Composite 3	90.042	23.808	13.080 ± 0.125	0.549 ± 0.005

The same dye removal experiment was also performed on Zr-Alg hydrogels and MOF-808 separately. As shown in Figure 4, composite **3** showed significantly higher MB uptake in aqueous solution compared to equivalent amounts of MOF-808 and hydrogels. In aqueous solution, composite **3** adsorbed 8.7 times more MB than the hydrogel and 6.5 times more MB than MOF-808. PC was also used to compare the performance of different materials, which yielded an adsorption for composite **3** that was 21.5 times higher than the hydrogel and 14.3 times higher than MOF-808 (Table 2). This demonstrates the effect of PC as a metric to further delineate calculated values and supports our assessment of the enhanced loading capacity of composite **3**. To the best of our knowledge, composite **3** exhibited the highest reported adsorption capacity of MB in aqueous solution among the same class of materials.[42] A recent study of a cobalt MOF-alginate hydrogel hybrid reported adsorption kinetics parameters yielding an adsorption capacity of 87.387 mg/g for tetracycline at our initial adsorbate concentration, which can be compared with composite **3** adsorption of 88.866 mg MB/g sample (when adsorption is calculated per g dry weight sample rather than per g Zr content).[43] We hypothesized that the high adsorption capacity of composite **3** can be attributed to the combination of micropores from the MOF component and mesopores from the hydrogel component, in which the micropores create more surfaces to interact with/adsorb guest molecules while the mesopores facilitate the diffusion of guest molecules into the hybrid voids. Compared to MOF-808, the relatively larger voids in composite **3** also allow it to accommodate more MB molecules per mol of zirconium content. Essentially, the adsorption performance of the MOF-hydrogel hybrid is superior to the MOF (i.e. MOF-808) and the hydrogel (i.e. Zr-Alg hydrogel) alone, rendering its potential applications in MB delivery for bioimaging purposes and/or the removal of excess MB following administration.

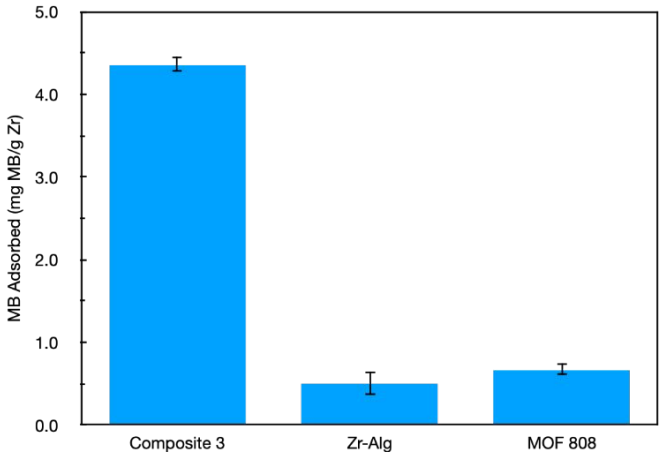

Figure 4 Methylene blue adsorption capacities of composite **3**, Zr-Alg hydrogel, and MOF-808 at 30.014uM initial MB concentration and pH 7 (all samples performed in triplicate, shown as average with standard deviation for error).

Table 2 PC comparison for methylene blue adsorption capacities of composite **3**, Zr-Alg hydrogel, and MOF-808 at 30.014uM initial MB concentration and pH 7 (all samples performed in triplicate, shown as average with standard deviation for error).

Sample	Final Concentration (uM MB)	MB Adsorbed (mg MB/g Zr)	PC (mg/g/uM)
Composite 3	25.326	4.361 ± 0.091	0.172 ± 0.004
Zr-Alg	64.798	0.502 ± 0.142	0.008 ± 0.002
MOF-808	57.731	0.672 ± 0.066	0.012 ± 0.001

We also sought to investigate the MB adsorption behaviors of obtained materials under different pH, expecting that the independent pH-sensitive behaviors of the hydrogel and MOF-808 would interpolate to produce unique adsorption properties of the composite. Alginate hydrogels are expected to undergo a reduction in osmotic pressure upon protonation of uncoordinated carboxylates around a pH of 3.0-3.5, resulting in expulsion of water from the pores.[53] Meanwhile, the trimesic acid linkers can dissociate from Zr ions above pH 7.4, causing partial collapse of MOF-808.[23] As shown in Figure 5, the Zr-Alg hydrogels showed increased MB adsorption under pH 1.3, possibly due to their greater electrostatic interaction with dye molecules upon hydrogel shrinking in acidic conditions.[51,54,55] When placed in a pH 1 solution, the hydrogel may have compressed to an extent that caused steric constraint for MB encapsulation, hence a lower MB adsorption was observed. In comparison, MOF-808 showed very little response to increasing solution acidity for MB loading because MOF-808 is stable in acids and its rigid three-dimensional structure remained unchanged.[23,56] Interestingly, composite **3** showed incrementally decreasing adsorption of MB as the pH was decreased. The MB adsorption capacity of composite **3** under acidic conditions may be impacted by the loss of mesopore-facilitated dye diffusion as the hydrogel component shrank to closer proximity to the MOF-like micropores, possibly blocking certain adsorption sites.[55] Upon exposure to basic conditions, Zr-Alg hydrogels showed slightly increased MB loading capacity, likely resulting from some enhanced dye diffusion in the expanded hydrogel mesopores. We think the significantly enhanced encapsulation of MB by MOF-808 under pH 13 is due to the instability of the MOF in base,[23] which led to missing linker/node defects exposing uncoordinated carboxylates within the MOF micropores and stimulating a higher negative surface charge.[57] The electrostatic interaction with positively charged MB molecules was therefore increased under basic conditions. In fact, the adsorption capacity of MB in the partially decomposed MOF-808 (in base) was similar to that of composite **3** in neutral pH. On the other hand, composite **3** adsorbed slightly less MB under basic pH, possibly due to the local decomposition of the MOF components in the composite caused by linker dissociation.[23] Within the range of pH 5.5-8.5, the loading capacity of the composite remained largely unchanged, demonstrating its excellent chemical stability. These experiments further indicated that the MOF-hydrogel hybrid (composite **3**) inherited properties of both the MOF and the hydrogel. While possessing both the micropores from the MOF and the mesopores from the hydrogel, the composite also presented similar stability of the MOF and flexibility of the hydrogel, giving rise to its unique pH-dependent adsorption behaviors.

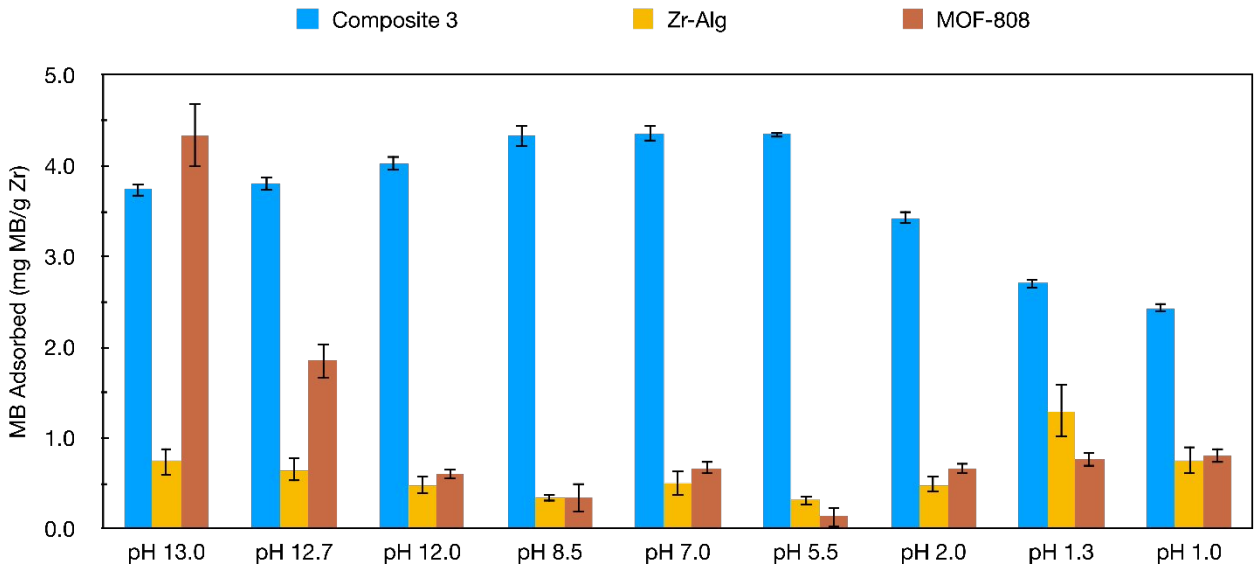

Figure 5 Methylene blue adsorption capacity of synthesized materials (composite **3** in blue, Zr-Alg hydrogel in yellow, and MOF-808 in brown) in solutions of varied pH (all samples performed in triplicate, shown as average with standard deviation for error).

In addition to varying pH, the response of obtained materials to increasing ionic strength was also explored. The selected NaCl concentrations were based on previously documented adsorption responses for alginate hydrogels.[58] Given the free carboxylates dispersed throughout the hydrogel structure, Zr-Alg was expected to swell in response to ion addition. As shown in Figure 6, this swelling yielded improved hydrogel loading capacity at the highest NaCl concentration. MOF-808 similarly underwent an increase in MB loading as ionic strength was increased. Several MOFs with carboxylate linkers have been shown to effectively encapsulate NaCl,[59] therefore, the observed response of MOF-808 to ionic strength may be the result of adding ionic interactions between MB and NaCl encapsulated in MOF pores. On the other hand, within error, composite **3** showed no change in loading capacity, maintaining its high MB adsorption compared with the other materials. This property may prove useful for reducing leakage in applications as a biomaterial, given that medical saline is typically 0.154M NaCl and physiological salt concentrations can be dynamic.

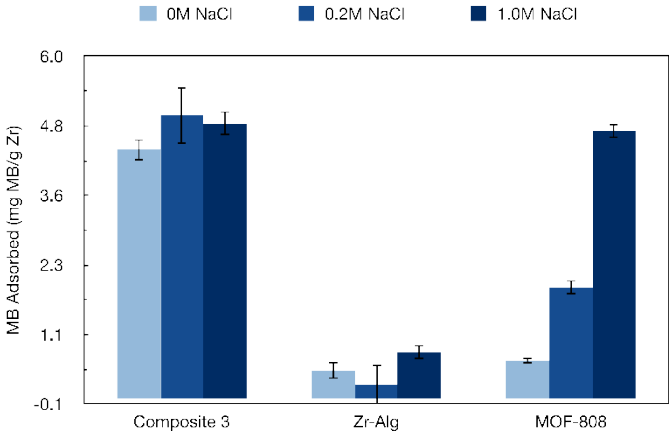

Figure 6 Methylene blue adsorption capacity of synthesized materials in solutions with varied ionic strength (0.2M NaCl in dark blue and 1.0M NaCl in light blue).

Overall, composite **3** broadly retained a greater adsorption capacity for MB compared to the hydrogel and MOF-808 within the tested conditions (pH 1-13, 0.2-1.0 M NaCl), demonstrating its enhanced adsorptive performance and excellent chemical stability. Low doses of MB can be administered for bioimaging or guided surgery; however, excess dosing of MB can lead to skin lesions and neurotoxic effects.[60-62] The high adsorption capacity of composite **3** and its stability in varying pH/ionic strength makes it a promising material for topical or circulatory removal of free MB dyes that are not bound to target tissue/tumor post-administration, thereby preventing adverse effects caused by excess MB.

Conclusions

A MOF-hydrogel hybrid, Zr-MOF-Alg (composite **3**), was synthesized via a green chemistry approach, and this hybrid exhibited enhanced performance compared to individual Zr-Alg hydrogels and MOF-808, particularly in near-neutral pH ranges.

Taking advantage of the hydrophilicity and biocompatibility of alginate hydrogels as well as the highly porous nature of MOFs, this new hybrid material was developed with properties that are suitable for biomedical applications. Importantly, composite **3** exhibited the highest reported adsorption capacity of the MB dye in aqueous solution among the same class of hybrids, and it displayed greater retention of its loading capacity across a wide pH range (pH 1 to 13) and NaCl concentration (0.2-1.0 M) compared to the constituent materials. The excellent loading capacity and chemical stability of the composite endow it with the ability to efficiently adsorb MB in dynamic environments. Particularly, it may be of interest as a novel platform for the removal of MB contrast dye following guided surgery or tumor imaging to prevent adverse side effects of excess MB. Future work may focus on nanosizing the Zr-MOF-Alg composites and exploring their efficacy in delivering/removing therapeutics as well as dye molecules for bioimaging.

Conflicts of interest

There are no conflicts to declare.

Acknowledgements

The authors gratefully acknowledge the NSF funded Partnership for Research and Education in Materials (PREM) at CSULA (DMR 1523588). Acknowledgement is also made to the donors of the American Chemical Society Petroleum Research Fund for partial support of this research (57951-UNI10). S.E.K. acknowledges support from the REU program at the Pennsylvania State University (DMR1460920, DMR 1420620, and DMR1523588). J.D.S. and Y.L. acknowledge support from NSF-CREST program (HRD 1547723 and Amendment 003). W.I.F. was supported by the National Institute of General Medical Sciences of the National Institute of Health under Award Number GM08228. S.E.K. acknowledges guidance from Tawanda Zimudzi at Pennsylvania State University for analysis of FTIR results.

References

1 Wu, W.; Aiello, M.; Zhou, T.; Berliner, A.; Banerjee, P.; Zhou, S. In-situ immobilization of quantum dots in polysaccharide-based nanogels for integration of optical pH-sensing, tumor cell imaging, and drug delivery. *Biomaterials,* 2010, **31** (11), 3023–3031.

2 Ikada, Y.; Iwata, H.; Horii, F.; Matsunaga, T.; Taniguchi, M.; Suzuki, M.; Taki, W.; Yamagata, S.; Yonekawa, Y.; Handa, H. Blood compatibility of hydrophilic polymers. *J. Biomed. Mater. Res.* 1981, **15** (5), 697-718.

3 Kato, Y.; Ozawa, S.; Miyamoto, C.; Maehata, Y.; Suzuki, A.; Maeda, T.; Baba, Y. Acidic extracellular microenvironment and cancer. *Cancer Cell Int.* 2013, **13**, 89.

4 Vlahov, I.R.; Leamon, C.P. Engineering folate-drug conjugates to target cancer: from chemistry to clinic. *Bioconjugate Chem.* 2012, **23** (7), 1357-1369.

5 Sur, S.; Fries, A.C.; Kinzler, K.W.; Zhou, S.; Vogelstein, B. Remote loading of preencapsulated drugs into stealth liposomes. *Proc. Natl. Acad. Sci. USA* 2014, **111** (6), 2283-2288.

6 Li, J.; Mooney, D.J. Designing hydrogels for controlled drug delivery. *Nat. Rev. Mater.* 2016, **1**, 16071.

7 Baeza, A.; Ruiz-Molina, D.; Vallet-Regi, M. Recent advances in porous nanoparticles for drug delivery in antitumoral applications: inorganic nanoparticles and nanoscale metal-organic frameworks. *Expert Opin. Drug Deliv.* 2017, **14** (6), 783-796.

8 Thurn, K.T.; Brown. E.; Wu, A.; Vogt, S.; Lai, B.; Maser, J.; Paunesku, T.; Woloschak, G.E. Nanoparticles for applications in cellular imaging. *Nanoscale Res. Lett.* 2007, **2** (9), 430-441.

9 Lu, J.; Liong, M.; Li, Z.; Zink, J.I.; Tamanoi, F. Biocompatibility, biodistribution, and drug-delivery efficiency of mesoporous silica nanoparticles for cancer therapy in animals. *Small* 2010, **6** (16), 1794-1805.

10 Longmire, M.; Choyke, P.L.; Kobayashi, H. Clearance properties of nano-sized particles and molecules as imaging agents: considerations and caveats. *Nanomedicine* 2008, **3** (5), 703-717.

11 Zhang, X.; Liang, Q.; Han, Q.; Wan, W.; Ding, M. Metal-organic frameworks@ graphene hybrid aerogels for solid-phase extraction of non-steroidal anti-inflammatory drugs and selective enrichment of proteins. *The Analyst* 2016, **141** (13), 4219–4226.

12 Ulker, Z.; Erkey, C. An emerging platform for drug delivery: Aerogel based systems. *J. Control Release* 2014, **177**, 51-63.

13 Sumida, K.; Liang, K.; Reboul, J.; Ibarra, I. A.; Furukawa, Falcaro, P. Sol-gel processing of metal-organic frameworks. *Chem. Mater.* 2017, **29** (7), 2626–2645.

14 Owens, G.J.; Singh, R.K.; Foroutan, F.; Alqaysi, M.; Han, C.-M.; Mahapatra, C.; Kim, H.-W.; Knowles, J.C. Sol-gel based materials for biomedical applications. *Prog. Mater. Sci.* 2016, **77**, 1-79.

15 Servatan, M.; Zarrintaj, P.; Mahmodi, G.; Kim, S.-J.; Ganjali, M.R.; Saeb, M.R.; Mozafari, M. Zeolites in drug delivery: Progress, challenges and opportunities. *Drug Discov. Today* 2020, **25** (4), 642-656.

16 Wu, Q.; Niu, M.; Chen, X.; Tan, L.; Fu, C.; Ren, X.; Ren, J.; Li, L.; Xu, K.; Zhong, H.; Meng, X. Biocompatible and biodegradable zeolitic imidazolate framework/polydopamine nanocarriers for dual stimulus triggered tumor thermo-chemotherapy. *Biomaterials* 2018, **162**, 132-143.

17 Fleischmann, E.-K.; Zentel, R. Liquid-crystalline ordering as a concept in material science: from semiconductors to stimuli-responsive devices. *Angew. Chem. Int. Ed.* 2013, **52** (34), 8810–8827.

18 Jobbágy, C.; Deák, A. Stimuli-responsive dynamic gold complexes. *Eur. J. Inorg. Chem.* 2014, **2014** (27), 4434–4449.

19 Furukawa, H.; Cordova, K.; O'Keeffe, M.; Yaghi, O. The chemistry and applications of metal-organic frameworks. *Science* 2013, **341** (6149).

20 Zhou, H.; Long, J.; Yaghi, O. Introduction to metal-organic frameworks. *Chem. Rev.* 2012, **112** (2), 673–674.

21 Kim, M.; Cahill, J. F.; Su, Y.; Prather, K. A.; Cohen, S. M. Postsynthetic ligand exchange as a route to functionalization of 'inert' metal-organic frameworks. *Chem. Sci.* 2012, **3** (1), 126–130.

22 Farha, O. K.; Eryazici, I.; Jeong, N. C.; Hauser, B. G.; Wilmer, C. E.; Sarjeant, A. A.; Snurr, R. Q.; Nguyen, S. T.; Yazaydın, A. Ö.; Hupp, J. T. Metal-organic framework materials with ultrahigh surface areas: is the sky the limit? *J. Am. Chem. Soc.* 2012, **134** (36), 15016–15021.

23 Howarth, A. J.; Liu, Y.; Li, P.; Li, Z.; Wang, T. C.; Hupp, J. T.; Farha, O. K. Chemical, thermal and mechanical stabilities of metal-organic frameworks. *Nat. Rev. Mater.* 2016, **1** (3).

24 Senkovska, I.; Kaskel, S. Ultrahigh porosity in mesoporous MOFs: promises and limitations. *Chem. Commun.* 2014, **50** (54), 7089.

25 Orellana-Tavra, C.; Baxter, E. F.; Tian, T.; Bennett, T. D.; Slater, N. K. H.; Cheetham, A. K.; Fairen-Jimenez, D. Amorphous metal-organic frameworks for drug delivery. *Chem. Commun.* 2015, **51** (73), 13878–13881.

26 Liu, Y.; Howarth, A. J.; Vermeulen, N. A.; Moon, S.-Y.; Hupp, J. T.; Farha, O. K. Catalytic degradation of chemical warfare

agents and their simulants by metal-organic frameworks. *Coord. Chem. Rev.* 2017, **346**, 101–111.
27 Mondloch, J. E.; Katz, M. J.; Isley, W. C.; Ghosh, P.; Liao, P.; Bury, W.; Wagner, G. W.; Hall, M. G.; DeCoste, J. B.; Peterson, G. W.; Snurr, R. Q.; Cramer, C. J.; Hupp, J. T.; Farha, O. K. Destruction of chemical warfare agents using metal-organic frameworks. *Nat. Mater.* 2015, **14** (5), 512–516.
28 Millward, A. R.; Yaghi, O. M. Metal-organic frameworks with exceptionally high capacity for storage of carbon dioxide at room temperature. *J. Am. Chem. Soc.* 2005, **127** (51), 17998–17999.
29 Dhakshinamoorthy, A.; Asiri, A. M.; García, H. Metal-organic framework (MOF) compounds: photocatalysts for redox reactions and solar fuel production. *Angew. Chem. Int. Ed.* 2016, **55** (18), 5414–5445.
30 Samanta, D.; Roy, S.; Sasmal, R.; Saha, N.D.; R, P.K.; Viswanatha, R.; Agasta, S.S.; Maji, T.K. Solvent adaptive dynamic metal-organic soft hybrid for imaging and biological delivery. Angew. *Chem. Int. Ed. Engl.* 2019, **58** (15), 5008-5012.
31 Sun, C.-Y.; Qin, C.; Wang, X.-L.; Su, Z.-M. Metal-organic frameworks as potential drug delivery systems. *Expert Opin. Drug Deliv.* 2013, **10** (1), 89-101.
32 Veronese, F.M. Peptide and protein PEGylation: a review of problems and solutions. *Biomaterials* 2001, **22** (5), 405-417.
33 Liu, H.; Zhu, H.; Zhu, S. Reversibly dispersible/collectable metal-organic frameworks prepared by grafting thermally responsive and switchable polymers. *Macromol. Mater. Eng.* 2014, **300** (2), 191–197.
34 Mao, Y.; Li, J.; Cao, W.; Ying, Y.; Sun, L.; Peng, X. Pressure-assisted synthesis of HKUST-1 thin film on polymer hollow fiber at room temperature toward gas separation. *ACS Appl. Mater. Interfaces* 2014, **6** (6), 4473–4479.
35 Rodenas, T.; Luz, I.; Prieto, G.; Seoane, B.; Miro, H.; Corma, A.; Kapteijn, F.; Xamena, F. X. L. I.; Gascon, J. Metal-organic framework nanosheets in polymer composite materials for gas separation. *Nat. Mater.* 2014, **14** (1), 48–55.
36 Qiu, S.; Xue, M.; Zhu, G. Metal-organic framework membranes: from synthesis to separation application. *Chem. Soc. Rev.* 2014, **43** (16), 6116–6140.
37 Huo, J.; Marcello, M.; Garai, A.; Bradshaw, D. MOF-polymer composite microcapsules derived from pickering emulsions. *Adv. Mater.* 2013, **25** (19), 2717–2722.
38 Sabetghadam, A.; Seoane, B.; Keskin, D.; Duim, N.; Rodenas, T.; Shahid, S.; Sorribas, S.; Guillouzer, C. L.; Clet, G.; Tellez, C.; Daturi, M.; Coronas, J.; Kapteijn, F.; Gascon, J. Metal organic framework crystals in mixed-matrix membranes: impact of the filler morphology on the gas separation performance. *Adv. Funct. Mater.* 2016, **26** (18), 3154–3163.
39 Basu, S.; Cano-Odena, A.; Vankelecom, I. F. Asymmetric matrimid®/[Cu3 (BTC) 2] mixed-matrix membranes for gas separations. *J. Membrane Sci.* 2010, **362** (1-2), 478–487.
40 Hwang, S.; Chi, W. S.; Lee, S. J.; Im, S. H.; Kim, J. H.; Kim, J. Hollow ZIF-8 nanoparticles improve the permeability of mixed matrix membranes for CO2/CH4 gas separation. *J. Membrane Sci.* 2015, **480**, 11–19.
41 Bueken, B.; Velthoven, N. V.; Willhammar, T.; Stassin, T.; Stassin, I.; Keen, D. A.; Baron, G. V.; Denayer, J. F. M.; Ameloot, R.; Bals, S.; De Vos, D.; Bennett, T. D. Gel-based morphological design of zirconium metal-organic frameworks. *Chem. Sci.* 2017, **8**, 3939–3948.
42 Zhu, H.; Zhang, Q.; Zhu, S. Alginate hydrogel: A shapeable and versatile platform for *in situ* preparation of metal-organic framework-polymer composites. *ACS Appl. Mater. Interfaces* 2016, **8** (27), 17395–17401.
43 Zhuang, Y.; Kong, Y.; Wang, X.; Shi, B. Novel one step preparation of a 3D alginate based MOF hydrogel for water treatment. *New J. Chem.* 2019, **43**, 7202-7208.
44 Xiao, J.; Chen, S.; Yi, J.; Zhang, H. F.; Ameer, G. A. A cooperative copper metal-organic framework-hydrogel system improves wound healing in diabetes. *Adv. Funct. Mater.* 2016, **27** (1), 1604872.
45 Mao, J.; Ge, M.; Huang, J.; Lai, Y.; Lin, C.; Zhang, K.; Meng, K.; Tang, Y. Constructing multifunctional MOF@ rGO hydro-/aerogels by the self-assembly process for customized water remediation. *J. Mater. Chem. A* 2017, **5** (23), 11873–11881.
46 Ishiwata, T.; Furukawa, Y.; Sugikawa, K.; Kokado, K.; Sada, K. Transformation of metal-organic framework to polymer gel by cross-linking the organic ligands preorganized in metal-organic framework. *J. Am. Chem. Soc.* 2013, **135** (14), 5427–5432.
47 Yasasvini, S.; Anusa, R.S.; VedhaHari, B.N.; Prabhu, P.C.; RamyaDevi, D. Topical hydrogel matrix loaded with simvastatin microparticles for enhanced wound healing activity. *Mater. Sci. Eng. C. Mater. Biol. Appl.* 2017, **72**, 160-167.
48 Zhang, Z.; Kim, Y.; Song, S. Injectable and quadruple-functional hydrogel as an alternative to intravenous delivery for enhanced tumor targeting. *ACS Appl. Mater. Interfaces* 2019, **11** (38), 34634-34644.
49 Hah, H.J.; Kim, G.; Lee, Y.-E.K.; Orringer, D.A.; Sagher, O.; Philbert, M.A.; Kopelman, R. Methylene blue-conjugated hydrogel nanoparticles and tumor-cell targeted photodynamic therapy. *Macromol. Biosci.* 2011, **11**, 90-99.
50 Tummers, Q.R.J.G.; Verbeek, F.P.R.; Schaafasma, B.E.; Boonstra, M.C.; van der Vorst, J.R.; Liefers, G.-J.; van de Velde, C.J.H.; Frangioni, J.V.; Vahrmeijer, A.L. Real-time intraoperative detection of breast cancer using near-infrared fluorescence imaging and methylene blue. *Eur. J. Surg. Onc.* 2014, **40** (7), 850-858.
51 Furukawa, H.; Gándara, F.; Zhang, Y.-B.; Jiang, J.; Queen, W. L.; Hudson, M. R.; Yaghi, O. M. Water adsorption in porous metal-organic frameworks and related materials. *J. Am. Chem. Soc.* 2014, **136** (11), 4369–4381.
52 O'Connor, D.J.; Connolly, J.P. The effect of concentration of adsorbing solids on the partition coefficient. *Water Res.* 1980, **14** (10), 1517-1523.
53 Qiusheng, Z.; Xiaoyan, L.; Jin, Q.; Jing, W.; Xuegang, L. Porous zirconium alginate beads adsorbent for fluoride adsorption from aqueous solutions. *RSC Adv.* 2015, **5** (3), 2100–2112.
54 Rizwan, M.; Yahya, R.; Hassan, A.; Yar, M.; Azzahari, A.; Selvanathan, V.; Sonsudin, F.; Abouloula, C. pH sensitive hydrogels in drug delivery: Brief history, properties, swelling, and release mechanism, material selection and applications. *Polymers* 2017, **9** (12), 137.
55 Jiang, J.; Gándara, F.; Zhang, Y.-B.; Na, K.; Yaghi, O. M.; Klemperer, W. G. Superacidity in sulphated metal-organic framework-808. *J. Am. Chem. Soc.* 2014, **136** (37), 12844–12847.
56 Efome, J. E.; Rana, D.; Matsuura, T.; Lan, C. Q. Metal-organic frameworks supported on nanofibers to remove heavy metals. *J. Mater. Chem. A* 2018, **6** (10), 4550–4555.
57 Chuang, J.-J.; Huang, Y.-Y.; Lo, S.-H.; Hsu, T.-F.; Huang, W.-Y.; Huang, S.-L.; Lin, Y.-S. Effects of pH on the shape of alginate particles and its release behavior. *Int. J. Polym. Sci.* 2017, **2017**, 1–9.
58 Zhang, K.; Luo, Y.; Li, Z. Synthesis and characterization of a pH- and ionic strength-responsive hydrogel. *Soft Mater.* 2007, **5**(4), 183-195.
59 Ou, R.; Zhang, H.; Wei, J.; Kim, S.; Wan, L.; Nguyen, N.S.; Hu, Y.; Zhang, X.; Simon, G.P.; Wang, H. Thermoresponsive amphoteric metal-organic frameworks for efficient and reversible adsorption of multiple salts from water. *Adv. Mater.* 2018, **30** (34), 1802767.
60 Stradling, B.; Aranha, G.; Gabram, S. Adverse skin lesions after

methylene blue injections for sentinel lymph node localization. *Am. J. Surg.* 2002, **184** (4), 350-352.

61 Vutskits, L.; Briner, A.; Klauser, P.; Gascon, E.; Dayer, A.G.; Kiss, J.Z.; Muller, D.; Licker, M.J.; Morel, D.R. Adverse effects of methylene blue on the central nervous system. *Anesthesiology* 2008, **108** (4), 684-692.

62 Guler, S.A.; Kirnaz, S.; Simsek, T.; Demir, C.I.; Gunes, A.; Isken, T.; Canturk, N.Z.; Utkan, N.Z. Cutaneous adverse effects of methylene blue in an animal skin-flap model. *Acta. Chirurgica Belgica* 2020, **120** (3), 167-172.